NORWEGIAN UNIVERSITY OF SCIENCE AND TECHNOLOGY
DEPARTMENT OF PHYSICS

SUGGESTED SOLUTION TO EXAM I COURSE
TFY 4310 MOLECULAR BIOPHYSICS
Saturday 18. december 2010
Time: kl. 0900 – 1300.

EXERCISE 1

a) sp-, sp^2- and sp^3-orbitals are hybridized orbitals of the atomic s and p orbitals involved in covalent bonding. They can be seen as linear combinations of the s and p orbitals localized at the same nuclei, and can generally be written

$$\Psi = \alpha_1 \Psi_{ns} + \alpha_2 \Psi_{np_x} + \alpha_3 \Psi_{np_y} + \alpha_4 \Psi_{np_z}$$

sp^3-orbitals: Coefficients α_1 α_2, α_3 and α_4 are all non-zero. Found e.g. in metan (CH_4) and ethanol (H_3CCHOH).
sp^2-orbitals: $\alpha_1 = 1$. Two of the coefficients α_2, α_3 and α_4 are non-zero and the third is equal to zero. Found e.g. in $H_2C=CH_2$ and graphene.
sp-orbitals: $\alpha_1 = 1$, and one of the coefficients α_2, α_3 and α_4 is non-zero and the rest equals zero. Found e.g. in acetylen HCCH.

b) H_2O contains a total of 10 electrons. Two of these are locate in a 1s non-bonding orbital of the O-atom. Four of the remaining electrons are located in two sp^3 non-binding electron tails and the remaining four in the two s-sp^3-σ-bonds between the oxygen atom and the two hydrogen atoms (Figure 1).An electron tail is e.g. a sp^3 orbital that contains two electrons, but is not part of and covalent bond (Figure 1).
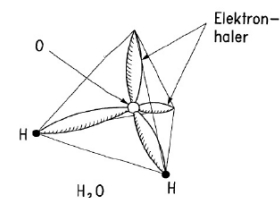

Figure 1. Schematic illustration of structure of water molecule

The interaction between the highly polar O-H bond and the electrons in hydrogen in a H-C bond is an example of a hydrogen bond. The energy of the bond in to a large extent due to electrostatic interaction, but there is also a significant contribution that has quantum mechanical origin. Hydrogen bonds are weak bonds compared to covalent bonds.

A model where H_2O can be viewed as a highly dynamic ice slurry where the lifetime of a given hydrogen bond is about 10^{-11} seconds and average size of the "ice pieces"is just a few nanometers can account for the observed large fraction of the hydrogen bonds (85%) in water compared to ice. This often also referred to as a system consisting of fluctuating clusters. At any time there is in average only app. 15% of the water molecules that are free water molecules. Lifetime of H2O molecule cluster membership (10^{-11} s) and cluster size decreases with T. Cluster size: from 90 (2degC) to 25 at 90 degC
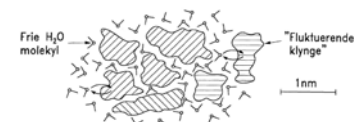

Figure 2. Fluctuating cluster model for water

c)   The hydrofobic effect (interactions/bonds) is connected to the fact that it is energetically favourable for water molecules to form more regular structures near apolar surfaces than in free aqueous solution. This ordering, however, is entropically unfavorable. When two such apolar surfaces with structured water molecules are brought together, the apolar surfaces will not be accessible for
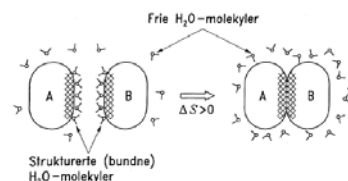

Figure 3. Schematic illustration of entropy gain of water occurring on association of apolar surfaces

structuring of water molecules, and thus, a larger fraction of the water is not stuctured. Or in other words: the association of the apolar surfaces is driven by an entropy gain in the aqueous system.

Hydrofobic interactions contribute to the molecular organisation of the red blood cell membrane (Figure 4) in three main ways: The first is the stability of the lipid bilayer where the hydrophobic effect underpins the assembly to the lipid molecules in the bilayer. Here, the aliphatic tail of the lipid molecules is found in the internal part of the bilayer, and the polar/charged groups of the lipids faces towards the external aqueous phase. The second contribution of the hydrophobic effect is to the organisation of the individual protein molecules, where in particular the globular organisation is recognized with a

Figure 4. Schematic illustration of molecular organisation of the cell membrane of red blood cells. The illustration shows a cross-section.

hydrophobic interior. The third area where the hydrophobic effect is taking part in organizing the cell membrane is the correct positioning of the transmembrane proteins in the lipid bilayer. The orientation of such proteins in the membrane can be understood by a hydrophobic patch of the protein surface embedded in the hydrophobic interior of the lipid bilayer, whereas the more polar/charged parts of the protein is found sticking out from the surfaces of the lipid bilayer.
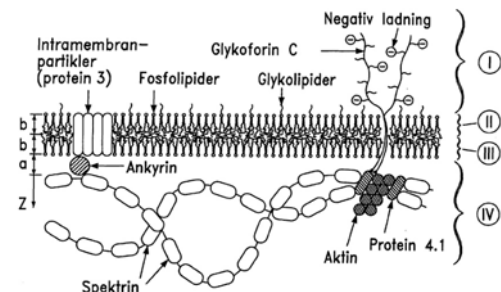
EXERCISE 2

a) The various components of the experimental setup for transient electric birefringence is identified in Figure 5. The biopolymer sample, often assymetric molecules (illustrated as rods in Fig 6), is located in the sample cell (Kerr cell, Fig 5). The Kerr cell is equipped with electrodes that are connected to a pulse generator. This is used to align the molecules with their dipole (partially permanent, partially induced) along the electrical field in the Kerr cell (when a static potential is applied). The dynamics of the alignment of the biological macromolecules is determined optically using the laser, polariser, analyser and PM tube as well as the readout for the PM tube (oscilloscope). The oscilloscope is also used to monitor the electric potential setup by the puls-generator on the Kerr cell. The optical detection is based on detection of orientation birefringe of the biological macromolecules. The optical conficuration consist of a monochromatic light source (laser) sendt through a polarizing filter (polarizer) with polarization axis oriented 45 deg relative to the electrical field in the Kerr cell. The light transmitted through the sample cell is analysed using an analyser (also polarizing filter) with crossed (90 deg) optical axis relative to the analyzer. The intensity of the
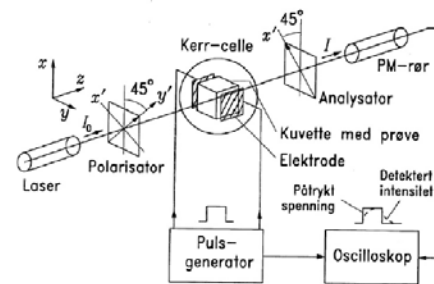

Figure 5. Schematic illustration of experimental setup for transient electric birefringence.
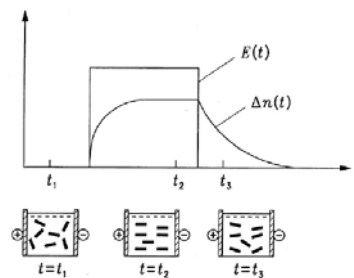
Figure 6. Schematic illustration of events in a typical TEB experiment.

light passing the analyzer is determined using the PM-tube (photomultiplier, alternatively and avalanche photodiode can be used). For isotropic distribution of macromolecular orientation, the solution is not birefringent, and I=0 is detected at the PM tube (t=t_1). In a typical experiment, the square pulse electrical potential that is applied to the Kerr cell for a certain (short) duration, induces orientation of the macromolecules (t=t_2, Fig 6). This is detected by the PM tube. Following shutting off the electrical potential, the molecules will reorient to an isotropic distribution with a time constant characterizing the

rotational properties of the molecules (t= t_3, Fig 6). The TEB setup can therefore be employed for determination of the rotational diffusion (or relaxation time) of the macromolecule. The equation:

$$I(t) = \frac{I_0}{4}\delta_0^2 \exp(-12 D_R t)$$

describes the basis for extracting the rotational diffusion constant D_R from the intensity data.

b) Figure 7 shows a schematic overview of an instrument suitable for static and dynamic light scattering. The main parts are: Light source with defined wavelength (laser), sample cuvette, thermostated bath for maintaining temperature, light detector mounted on a goniometer to detect light intensity at various angles $\tilde{\theta}$ Additionally, a computer properly interfacing to the various part for their control and data collection is usually included. A correlator is necessary for the dynamic light scattering experiments.
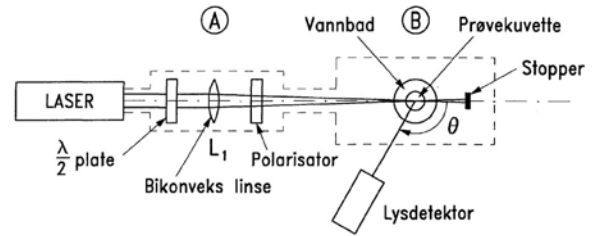

Figure 7. Schemativ illustration of instrument for light scattering.

Figure 8 shows the drawing that defines the scattering vector $\overrightarrow{\Delta k}$ as:

$$\overrightarrow{\Delta k} = \vec{k}_{ut} - \vec{k}_{in}$$

 The angle between the incident and the scattered wave vectors ($\vec{k}_{in}$ and $\vec{k}_{ut}$) is the scattering angle θ. The relation between the scattering vector and scattering angle is deduced from Fig 8b:

$$\left|\overrightarrow{\Delta k}\right| = 2\frac{2\pi}{\lambda_1}\sin(\theta/2) = \frac{4\pi}{\lambda_1}\sin(\theta/2)$$
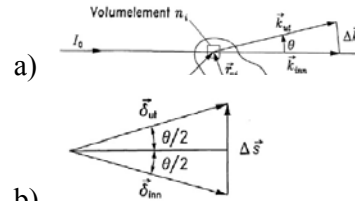

Figure 8. Schematic illustration of incident and scattered wave vectors ($\vec{k}_{in}$ and $\vec{k}_{ut}$) and scattering vector $\overrightarrow{\Delta k}$ (a) and the normalized wave vectors (b)

Inserted in $\quad \dfrac{\kappa c}{R_\theta} = \dfrac{1}{M}\left[1 + \dfrac{k^2}{3}R_G^2\right]\cdot[1+2B_2 c]$ **yields** $\quad \dfrac{\kappa c}{R_\theta} = \dfrac{1}{M}\left[1 + \dfrac{16\pi^2}{3\lambda_1^2}R_G^2 \sin^2\dfrac{\theta}{2}\right]\cdot[1+2B_2 c]$

Here:

$\kappa = \dfrac{4\pi^2 n_L^2 (d\tilde{n}/dc)^2}{N_A \lambda_0^4}$ is a constant for a particular solution, n_L is the refractive index of the solvent, $d\tilde{n}/dc$ the refractive index increment due to addition of macromolecule; N_A: avogadros constant, and λ_0 the wavelength of light in vacuum.

c is the macromolecular concentration, and R_θ the Rayleigh ratio ($R_\theta = I(\theta)r^2 / I_0$ for plan-polarized light, where r is the distance from the scattering event to the detector.). M is the molecular weight of the biomacromolecule, R_G the radius of gyration, and B_2 the second virial coefficient.

The molecular parameters that can be determined are the molecular weight (M), the radius of gyration (R_G) (and the second virial coefficient, B_2). Experimental data are analyzed according to the above eq, where a necessary experimental basis include determination of $I(\theta)$ for a range of θ, and for a set of concentrations c. The experimental data of $\kappa c/R_\theta$ is presented vs. $\sin^2 \theta/2 + Ac$, for each of the c and θ, and where A is a numerical constant. In this socalled Zimm-plot
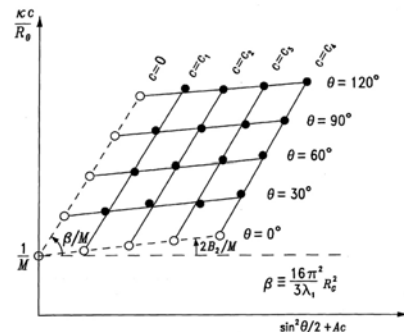

Figure 9. Zimm plot of light scattering data.

(Figure 9), the molecular weight is obtained as the inverse of the double extrapolation along the constant $\theta=0$ and c=0 extrapolated points. The radius of gyration is otained from the angular dependence of $\kappa c/R_\theta$ extrapolated to c=0. The second virial coefficient is obtained from the concentration depedence of $\kappa c/R_\theta$ extrapolated to $\theta=0$.

c) The chain model of a statistical chain is characterized by the lack of correlation between the directions of connected segments in a chain model. I.e.; in the chain segment model illustrated in Fig 10, consisting of N beads connected with totally N-1 connecting segment vectors of equal length, there is no correlation between the joining segments. We are assuming that all chain segments have the same length, Q, in the following. As a result, the probability distribution of the end-to-end vector is Gaussian, and the mean square end-to-end distance is given by:

Fig. 10. Chain segments of a polymer chain model

$$\langle r_{e-e}^2 \rangle = (N-1)Q^2$$

In the equivalent freely jointed chain, we replace N-1 by N_{eq} referring to the number of equivalent number (relative to chemical bonding structure) chain segments that can represent the chain. Thus: $\langle r_{e-e}^2 \rangle = N_e Q_e^2$ and the contour length is: $N_e Q_e = L_C$, where Q_e is the Kuhn segment length. From the given data for spectrin, we need to convert from radius of gyration, R_G, to $\langle r_{e-e}^2 \rangle$. With the above identification of the parameters, we have

$$\langle R_G^2 \rangle = \frac{1}{6}\frac{N+1}{N}\langle r_{e-e}^2 \rangle; \quad \text{that recasts to:} \quad \langle r_{e-e}^2 \rangle = 6\frac{N}{N+1}\langle R_G^2 \rangle = 6\frac{N_{eq}+1}{N_{eq}+2}\langle R_G^2 \rangle$$

The set of equations can either be solved iteratively in a numerical approach based on N_{eq} is large or directly without any assumptions regarding the magnitude of N_{eq}.

In the numerical approach based on the assumption that N_{eq} is large, thus $\langle r_{e-e}^2 \rangle \approx 6\langle R_G^2 \rangle$ is a reasonable approximation. Using this assumption, we get, $\dfrac{N_e Q_e^2}{N_e Q_e} = Q_e = \dfrac{\langle r_{e-e}^2 \rangle}{L_c} = \dfrac{6\langle R_G^2 \rangle}{L_c}$

Insertion of the numerical data in this formula, we get:

	Lc (nm)	R_G (nm)	Q_e (nm)	N_{eq}
Spectrin dimer	100	22	29.0	3.4
Spectrin tetramer	200	30	27.0	7.4

In this first approximation we observe that Q_e is not exactly the same for the estimates based on data for spectrin dimer and tetramer, N_{eq} for the estimate based on tetramer data not exactly twice of that for the dimer. This can still be within the precision that experimental data allow us to estimate such chain paratmeters, but note that the $\langle r_{e-e}^2 \rangle \approx 6\langle R_G^2 \rangle$ approximation is fullfilled to different extents for the two type of spectrin here. Since the assumption $\langle r_{e-e}^2 \rangle \approx 6\langle R_G^2 \rangle$ gives us the first estimate of N_{eq}, we can now perform a numerical iteration including N_{eq} in $\langle r_{e-e}^2 \rangle = 6\dfrac{N_{eq}+1}{N_{eq}+2}\langle R_G^2 \rangle$ to check possible convergence to one value of Q_e. Using this approach we get:

	0' approximation		1. iteration		2nd iteration	
	Q_e (nm)	N_{eq}	Q_e (nm)	N_{eq}	Q_e (nm)	N_{eq} (nm)
Spectrin dimer	29.0	3.4	23.7	4.2	24.4	4.1
Spectrin tetramer	27.0	7.4	24.1	8.2	24.4	8.2
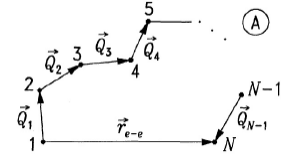
Thus, the calculation show that $Q_e = 24.4$ nm is an estimate of Kuhn segment length valid for both spectrin dimer and tetramer.

In the direct approach we are eliminating N_e from the relation between $\langle r_{e-e}^2 \rangle$ and radius of gyration:

$$6\langle R_G^2 \rangle = \frac{N_{eq}+2}{N_{eq}-1}\langle r_{e-e}^2 \rangle = \frac{N_{eq}+2}{N_{eq}-1}N_{eq}Q_e^2 = \frac{\frac{L_c}{Q_e}+2}{\frac{L_c}{Q_e}-1}\frac{L_c}{Q_e}Q_e^2 = L_cQ_e\frac{L_c+2Q_e}{L_c-Q_e}$$

This is reorganized to a second order eq in Q_e containing experimental accessible parameters:

$$2L_cQ_e^2 + \left(L_c^2 - 6\langle R_G^2 \rangle\right)Q_e - 6\langle R_G^2 \rangle L_c = 0$$

The solution of this is:

$$Q_e = -\frac{1}{2}\frac{L_c^2 - 6\langle R_G^2 \rangle}{2L_c} + \frac{1}{2}\sqrt{\left(\frac{L_c^2 - 6\langle R_G^2 \rangle}{2L_c}\right)^2 + 12\langle R_G^2 \rangle}$$

Inserting the numerical values of the experimental data, we obtain:

	Lc (nm)	R_G (nm)	Q_e (nm)	N_{eq}
Spectrin dimer	100	22	24.30	4.1
Spectrin tetramer	200	30	24.36	8.2

The two strategies used here are also shown to give the same answer (only one is required for full score).

EXERCISE 3

a) The parameters in the equation:

$$V(r) = \frac{q_1}{4\pi\varepsilon}\frac{1}{r}\exp\left(-r/\lambda_D\right)$$

that describes the electrostatic potential ($V(r)$) of a point-charge q_1 immersed in an aqueous solution with added salt are: $V(r)$ spherical symmetric potential as function distance r from origin located in the point charge q_1, r distance, λ_D is the Debye shielding distance, and ε the permitivity of the solution. For a given point-charge, the electrostatic potential is screened by the λ_D parameter which is controlled experimentally by the ionic strength in the solution.

b) With the information in the exercise, we start from the given partition function:

$$Z_0 \propto \lambda_D \int_0^{\lambda_D} \left(r/\lambda_D\right)^{1+Z_iZ_p2\xi} dr \tag{3-1}$$

where the parameter ξ is given by:

$$\xi = \frac{e^2}{4\pi\varepsilon k_BTb} \tag{3-2}$$

The model considered of a stiff cylinder, have charged groups of valence Z_p at mutual distance b along the long axis of the cylinder. The concept of the counterion condensation emerges from the fact that the integral in eq. 3-1 need to converge to represent a physical system. The integral in eq. 3-1 diverges when $1 + Z_iZ_p2\xi \leq -1$; or: when $-Z_iZ_p\xi \geq 1$. Considering monovalent bound charges, e.g. $Z_p = 1$; and monovalent counterions; e.g. $Z_i = -1$, one get the result that integral will diverge when $\xi \geq 1$. Inserting the maximum value of ξ; $\xi = 1$ for convergence in eq. 3-2, we get an estimate for the b needed for convergence of the integral in the partition function:

$$b_{critical} = b(\xi = 1) = \frac{e^2}{4\pi\varepsilon k_B T \xi}\bigg|_{\xi=1} = \frac{e^2}{4\pi\varepsilon k_B T} \qquad (3\text{-}3)$$

In cases where the b parameter from the structural data is less than $b_{critical}$, counterion will condense on the structure so that the effective b is $b_{critical}$. This is the counterion condensation phenomena.

For DNA, the structure yields totally 20 charges per 3.4 nm (10 bp in the duplex, there is two charges per duplex, one for each phospate group). The structural axial advance, b, per charge for a stiff line charge model is therefore: b= 3.4nm/20 = 0.17 nm. This is much less than $b_{critical}$ =0.714 nm and counterions will therefore condense. The change in charge density will be from:

e/0.17 nm = 5.88 e nm^{-1}

to

e/0.714 nm = 1.4 e nm^{-1};

or a reduction to 23.8% of the charge density expected from the structural information.